



HAL
open science

Capacitance Computation of Multi-Turn Windings via Elementary Neighbor-Conductor Models

Carlos Valdivieso, Gérard Meunier, Brahim Ramdane, Johan Gyselinck, Christophe Guerin, Ruth Sabariego

► **To cite this version:**

Carlos Valdivieso, Gérard Meunier, Brahim Ramdane, Johan Gyselinck, Christophe Guerin, et al.. Capacitance Computation of Multi-Turn Windings via Elementary Neighbor-Conductor Models. IEEE Journal on Multiscale and Multiphysics Computational Techniques, 2021, 6, pp.125-131. 10.1109/JMMCT.2021.3119864 . hal-03625837

HAL Id: hal-03625837

<https://hal.science/hal-03625837>

Submitted on 21 Mar 2024

HAL is a multi-disciplinary open access archive for the deposit and dissemination of scientific research documents, whether they are published or not. The documents may come from teaching and research institutions in France or abroad, or from public or private research centers.

L'archive ouverte pluridisciplinaire **HAL**, est destinée au dépôt et à la diffusion de documents scientifiques de niveau recherche, publiés ou non, émanant des établissements d'enseignement et de recherche français ou étrangers, des laboratoires publics ou privés.

Capacitance Computation of Multi-turn Windings via Elementary Neighbor-Conductor Models

Carlos A. Valdivieso, Gerard Meunier, Brahim Ramdane, Johan Gyselinck, Christophe Guerin,
and Ruth V. Sabariego

Abstract—In this paper, we propose a homogenization technique for the terminal-capacitance computation of multi-turn windings in electrostatic finite-element methods. The approach is based on a characterization of the elementary zones where the electrical energy is concentrated. It is valid for conductors of arbitrary cross-section and packing with standard or fly-back connections and orthogonal or orthocyclic dispositions. The results of the homogenized approach present excellent agreement with those obtained by accurate but expensive finite-element models, wherein all turns and insulation layers are explicitly discretized, and by experimental validation.

Index Terms—Capacitive effect, finite element method, high frequency, homogenization, windings.

I. INTRODUCTION

RECENT developments in power electronics have led to a high increase in the switching frequency used in e.g., power converters (transformers and inductors) [1]. Multi-turn windings in these electromagnetic devices are subjected to considerable capacitive effects. These effects result in resonances that may enhance the performance of the device [2]. Conversely, undesired parasitic currents also appear within the insulation layers, which result in e.g., electromagnetic interference (EMI), low efficiency and thermal degradation of the insulation [3]. Therefore, a correct prediction of these capacitances is essential at the design stage.

Local and global approaches have been proposed in the literature for the prediction of the capacitive effect [4]. On the one hand, local approaches treat the parasitic capacitances at the conductor level. This often results in the resolution of the full-wave Maxwell equations [5]–[7], or approximations to them that account simultaneously for the inductive and capacitive effects [8]–[10]. On the other hand, global approaches attempt to calculate an equivalent terminal capacitance for the winding, which is the objective of this work.

Different analytical techniques already exist for the computation of the terminal capacitance; yet their application is

restricted, in most cases, to round conductors with a certain winding configuration [11]. For instance, approaches suitable for single-layer windings are proposed in [12]–[14]. Multi-layer windings have also been treated [15], [16], but these approaches usually disregard the capacitance between conductors of the same layer. More complex models include nonetheless both the capacitances between turns in the same and adjacent layers [1], [17]–[20], where the main difference among them concerns the definition of the electric field path, between the conductors, for the respective analytical integrals. Numerical methods have been used as well, particularly the finite-element (FE) method. Classically, the terminal capacitance is obtained through an electrostatic FE model in which the representation of each separate turn of the winding is required [21], [22]. In [23], a homogenization technique has already been proposed for the thin dielectric layers in the winding.

In this paper, we propose a homogenization approach for the computation of the terminal capacitance in electrostatic FE models. It exploits the periodicity of windings by using a 2-D elementary cell. Such cell aims at characterizing the concentration zones of electrostatic energy. The terminal capacitance is obtained through the stored energy in the cell and the winding terminal voltage. Conductors of arbitrary cross-section and packing, orthogonal or orthocyclic disposition, and standard or fly-back electrical connection can be treated with the proposed approach. Windings with round and rectangular conductors are considered in the application. A fine FE model for all cases, with all turns explicitly discretized, provides an accurate reference solution. Experimental results are also considered in the validations. The proposed approach can be applied to estimate the terminal capacitance of the windings comprised in devices such as: inductors, transformers, motors etc.

II. ELECTROSTATIC MODEL

A. Formulation

A bounded domain Ω of the Euclidean space is considered. For electrostatics problems, the electric field \underline{e} is expressed in terms of an electric scalar potential v , i.e.

$$\underline{e} = -\text{grad } v \text{ in } \Omega, \quad (1)$$

so that the Faraday equation is satisfied. The electric flux density \underline{d} is obtained from the constitutive relation, for linear isotropic materials, $\underline{d} = \varepsilon \underline{e}$, where ε is the scalar electric permittivity.

Manuscript received XXXX XX, 2021; revised XXXX XX, 2021. (Corresponding author: Carlos A. Valdivieso)

C. A. Valdivieso and C. Guerin are with Altair Engineering France, 38240 Meylan, France, F-38000 Grenoble, France (e-mail: cvaldivieso@altair.com; cguerin@altair.com).

G. Meunier and B. Ramdane are with the Université Grenoble Alpes, CNRS, Grenoble INP, G2Elab, F-38000 Grenoble, France (e-mail: gerard.meunier@grenoble-inp.fr; brahim.ramdane@grenoble-inp.fr).

J. Gyselinck is with the Department of Bio- Electro- And Mechanical Systems, Université Libre de Bruxelles, 1050 Brussels, Belgium (e-mail: johan.gyselinck@ulb.ac.be).

R. V. Sabariego is with the Department of Electrical Engineering, KU Leuven, 3600 Genk, Belgium (e-mail: ruth.sabariego@kuleuven.be).

For the electric scalar potential, a discrete FE function space $F_v(\Omega)$ is defined on a mesh of Ω containing the shape functions α_i and test functions α_j . The electrostatic formulation is then obtained from the weak form of Gauss' law for electric fields, i.e., find v such that

$$\int_{\Omega} \varepsilon \text{grad } v \cdot \text{grad } \alpha_j d\Omega = 0, \quad \forall \alpha_j \in F_v(\Omega), \quad (2)$$

with no free charges. The stored electrical energy W in Ω is obtained through the integral:

$$W = \frac{1}{2} \int_{\Omega} \varepsilon \underline{e}^2 d\Omega. \quad (3)$$

B. Winding Considerations

A winding of N_c periodically spaced turns and fill factor λ is considered. Each turn comprises a conductive part, or conductor, and the insulation, or dielectric, around it. Conductors are treated as perfect conductors (fixed uniform potentials) and the dielectric is assumed linear. The N_c turns are spatially distributed in N_l layers with N_t turns per layer, where N_t may vary from layer to layer. A linear distribution of the terminal voltage V_T is assumed across the winding with $N_c - 1$ independent voltages. In practice, such distribution is observed in small devices up to a frequency of 1 MHz [4].

The parasitic capacitance of a multi-turn and multi-layer winding depends on the wire parameters, the winding disposition and the electrical connection. Wire parameters concern the conductor shape and the dielectric properties of the insulation layers around it. The winding disposition specifies the spatial distribution of the winding layers. Two main winding dispositions are distinguished and considered hereafter: orthogonal and orthocyclic. In an orthogonal winding, the turns of adjacent layers lay on top of each other; whereas in an orthocyclic winding, the turns of adjacent layers lay in the gaps between two turns of the preceding layer. Fig. 1 shows the two types of winding dispositions. Evidently, the orthocyclic disposition (Fig. 1b) is inherent to round conductors. Windings with rectangular or square conductors are always orthogonal (Fig. 1a).

The electrical connection specifies the starting point of the consecutive winding layers. Two electrical connections are considered: fly-back and standard. In a fly-back connection, the starting point of the subsequent layer is fixed and corresponds to the starting point of the preceding layer. Inversely, in a standard connection, the starting point of the subsequent layer coincides with the end of the preceding one. In Fig. 1 fly-back and standard connections are associated to the orthogonal and orthocyclic windings, respectively.

Since the conductors have fixed imposed potentials, particular attention is paid to the resulting voltages between the turns. The turn-to-turn voltage V_{tt} defines the potential difference between two turns in the same layer and it is expressed, in terms of the terminal voltage V_T , as

$$V_{tt} = \frac{V_T}{N_c}. \quad (4)$$

Likewise, the layer-to-layer voltage defines the potential difference between two conductors of adjacent layers. Its definition depends on the winding disposition and the electrical

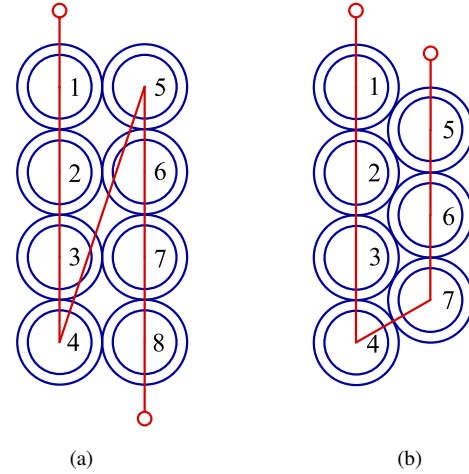


Fig. 1. Winding disposition and electrical connection: (a) Orthogonal winding with fly-back connection and (b) orthocyclic winding with standard connection.

connection. In that regard, only immediate neighboring turns are considered. Thus, in an orthogonal winding, the definition of the layer-to-layer voltage is straightforward and involves the two adjacent conductors in consecutive layers e.g., turns 1 and 5, 2 and 6... in Fig. 1a. As for the orthocyclic winding, we define it to represent an ascending pattern e.g., the voltages between turns 4 and 7, 3 and 6... in Fig. 1b.

In a winding with fly-back connection, the layer-to-layer voltage is always constant regardless of the turn position in the layer. In terms of the terminal voltage V_T , the fly-back layer-to-layer voltage V_{lf} is given by

$$V_{lf} = N_t \frac{V_T}{N_c}. \quad (5)$$

As for the standard connection, the layer-to-layer voltage is not constant and depends on the treated pair of turns p . Bottom-to-top wise for p in Fig. 1b, the standard layer-to-layer voltage V_{ls} reads:

$$V_{ls} = (2p - 1) \frac{V_T}{N_c}, \quad (6)$$

where $p = 1, 2, 3, \dots$ so that $p = 1$ accounts for turns 4 and 7, $p = 2$ for 3 and 6, etc. We consider hereafter orthocyclic windings with even-odd turns per layer (one turn difference between adjacent layers) as in Fig. 1b, where N_t corresponds to the lowest value of turns per layer.

III. ELEMENTARY NEIGHBOR-CONDUCTOR MODEL

Windings are by nature periodic structures (bundles of wires) and their capacitive effects may be accurately calculated with an equivalent elementary 2-D FE representation. Therefore, the complete electrostatic characterization of a winding can be carried out by means of an elementary cell comprising two or three conductors, as shown in Fig. 2, and the dielectric layers around them. Such cell represents the periodic zones where the electrical energy is concentrated throughout the winding. This way, only immediate neighboring turns are considered (both in a turn-to-turn and layer-to-layer basis) and the contribution of distant turns is assumed negligible.

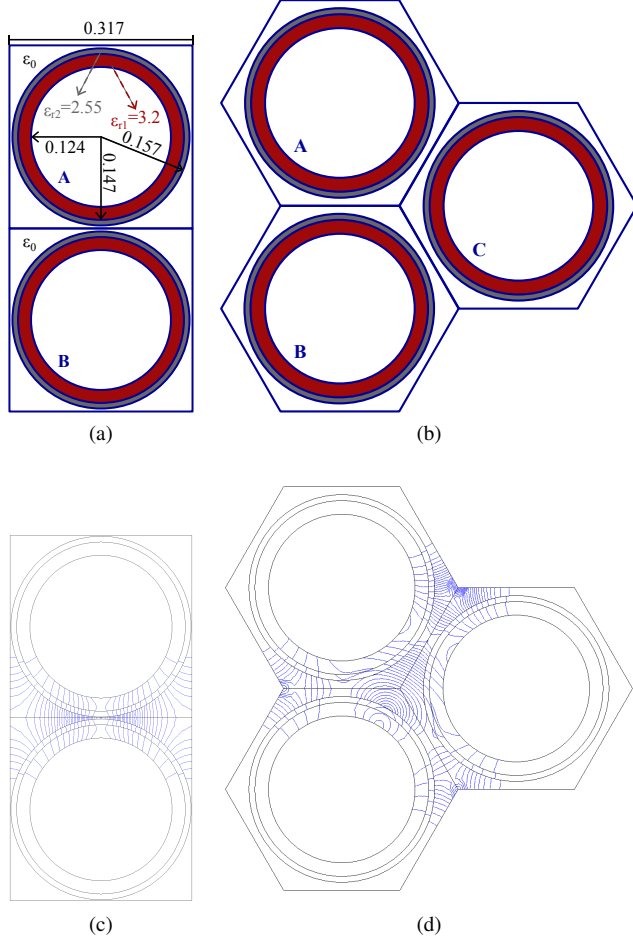


Fig. 2. Elementary 2-D cell for the electrostatic homogenization (dimensions: mm): (a) orthogonal disposition (b) orthocyclic disposition. Electric field lines: (c) orthogonal cell ($v_A = 2$ V and $v_B = 1$ V, with $V_{tt} = 1$ V) (d) orthocyclic cell ($v_A = 3$ V, $v_B = 2$ V and $v_C = 1$ V, with $V_{tt} = 1$ and $p = 1$).

The choice of the elementary cell depends on the winding disposition. Fig. 2 shows the cell for one of the conductors used hereafter in both orthogonal and orthocyclic dispositions. The conductor and insulation layers have radii: $r_c = 0.124$ mm, $r_1 = 0.147$ mm and $r_2 = 0.157$ mm, respectively, with fill-factor $\lambda = 0.48$. The relative electric permittivities of the insulation layers are: $\varepsilon_{r1} = 3.2$ and $\varepsilon_{r2} = 2.55$. In the orthogonal case (Fig. 2a), the cell comprises two winding turns embedded in an air-filled square packing. In the orthocyclic case (Fig. 2b), the cell contains additionally a third turn and features instead an air-filled square packing. At the resolution stage, the potentials v_A , v_B and v_C (corresponding to the conductive surfaces A , B and C in Fig. 2) are imposed, depending on the winding disposition and the electrical connection, together with floating potentials on the cell boundary.

If a winding is constructed by the spatial reproduction of the elementary cell, periodic conditions are guaranteed. In that case, the stored electrical energy in the winding W_w can be obtained from the stored electrical energy in the elementary cell by means of an energy balance. Such energy balance is based on the repetitions of the elementary cell across the winding. Thereon, the winding terminal capacitance C_w

is obtained based on the global redefinition of the stored electrical energy (3), i.e.

$$C_w = 2 \frac{W_w}{(V_T)^2}. \quad (7)$$

A. Orthogonal Winding Capacitance

In an orthogonal winding, the cell type in Fig. 2a can be used to account for both the turn-to-turn and layer-to-layer capacitive effects. Indeed, with round or square conductors, the geometry of the elementary cell in the turn-to-turn case is indistinct from the layer-to-layer case. In case of rectangular conductors, two different elementary cells are required for the turn-to-turn and layer-to-layer simulations given the asymmetry in the shape (see Fig. 4). Either way, with one or two elementary cells, we consider for all cases that

$$v_A - v_B = V_{tt}, \quad (8)$$

which leads the electric field distribution shown in Fig. 2c. Such condition results in the stored energies W_{tt} and W_{ll} for the turn-to-turn and layer-to-layer cases, respectively. Note that in the case of round and square conductors $W_{tt} = W_{ll}$.

1) *Fly-Back Connection*: The electrical connection determines the amount of energy stored within the layers of the winding. The electrostatic energy is proportional to the square value of the applied voltage, which allows the approximation of the stored energy in a fly-back winding as

$$W_w = N_l(N_t - 1)W_{tt} + N_t(N_l - 1) \left(\frac{V_{lf}}{V_{tt}} \right)^2 W_{ll}. \quad (9)$$

2) *Standard Connection*: The standard connection implies a changing behavior of the layer-to-layer stored energy, given the voltages between the turns of adjacent layers. Based on (6) and acknowledging again that electrostatic energy is proportional to the square value of the applied voltage, we define the stored energy in a standard winding as

$$W_w = N_l(N_t - 1)W_{tt} + (N_l - 1) \sum_{p=1}^{N_t} \left(\frac{V_{ls}}{V_{tt}} \right)^2 W_{ll}. \quad (10)$$

In (9) and (10), the first term in the right-hand side accounts for the of turn-to-turn repetitions and the second term for the layer-to-layer repetitions in the complete winding.

B. Orthocyclic Winding Capacitance

The elementary cell for the orthocyclic case is presented in Fig. 2b. In this cell, the turn-to-turn and layer-to-layer effects are estimated together. The potentials v_A and v_B preserve the condition in (8) and the stored electrical energy of the cell is denoted W_{tl} .

1) *Fly-Back Connection*: In a fly-back connection, the third potential v_C is defined as

$$v_C = v_B - V_{lf}. \quad (11)$$

In that way, both the turn-to-turn and layer-to-layer effects are included in the elementary cell. Since V_{lf} is constant, the stored energy in the winding is obtained through the number of cell repetitions over the domain, i.e.

$$W_w = N_t(N_l - 1)W_{tl}. \quad (12)$$

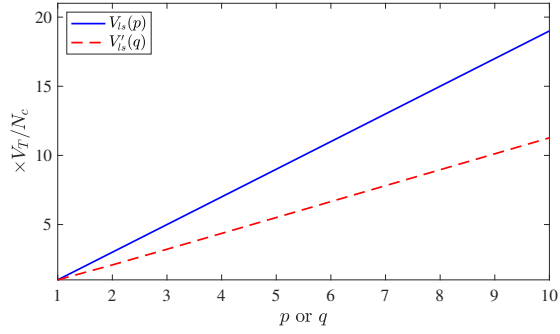


Fig. 3. Layer-to-layer voltage behavior vs pair p or trio q in an orthocyclic winding.

2) *Standard Connection*: The standard connection implies that the changing behavior of the layer-to-layer voltage has to be included in the cell. This can be easily achieved by imposing

$$v_C = v_B - V_{ls}, \quad (13)$$

which leads to the electric field distribution shown in Fig. 2d. For the sake of simplicity with a unique simulation, an expression in the form of (9) is required. Since the elementary cell comprises three turns, V_{ls} is not suitable. Nevertheless, the changing voltage in the elementary cell follows a linear behavior. Hence, a voltage V'_{ls} is defined to be a function of the involved trio of turns q (in the same way as V_{ls} is a function of p). By means of numerical simulations (see Appendix A), a general expression accounting for the linearity and the geometrical constraints of the orthocyclic cell is obtained. Bottom-to-top wise in fig. 1b, it reads:

$$V'_{ls} \simeq (1.1545q - 0.2708) \frac{V_T}{N_c}, \quad (14)$$

where $q = 1, 2, 3, \dots$. Thanks to the chosen even-odd repartition of the turns, V'_{ls} is valid for any set of three turns throughout the winding; provided that the shape of the elementary cell is maintained. Fig. 3 compares the layer-to-layer voltage behavior, treated by pairs or trios, in an orthocyclic winding as a function of the pair p or trio q . The energy stored in the winding is thus given by

$$W_w = (N_l - 1) \left(W_{tl} + \sum_{q=2}^{N_t} \left(\frac{V'_{ls}}{V_{tt}} \right)^2 W_{tl} \right). \quad (15)$$

Note that (9), (10), (12) and (15) are defined for complete windings with N_t turns per layer. However, incomplete windings can be treated as well provided that the contribution of the turns in the incomplete layers are added. Furthermore, axisymmetric windings may be treated with (9), (10), (12) and (15), provided that these energies are multiplied by the coordinate transformation factor:

$$\kappa = \pi(r_s + r_e), \quad (16)$$

where r_s and r_e are the winding starting and ending points over the r -direction. Note that the depth of the elementary cell in Cartesian coordinates is set to 1 m by default.

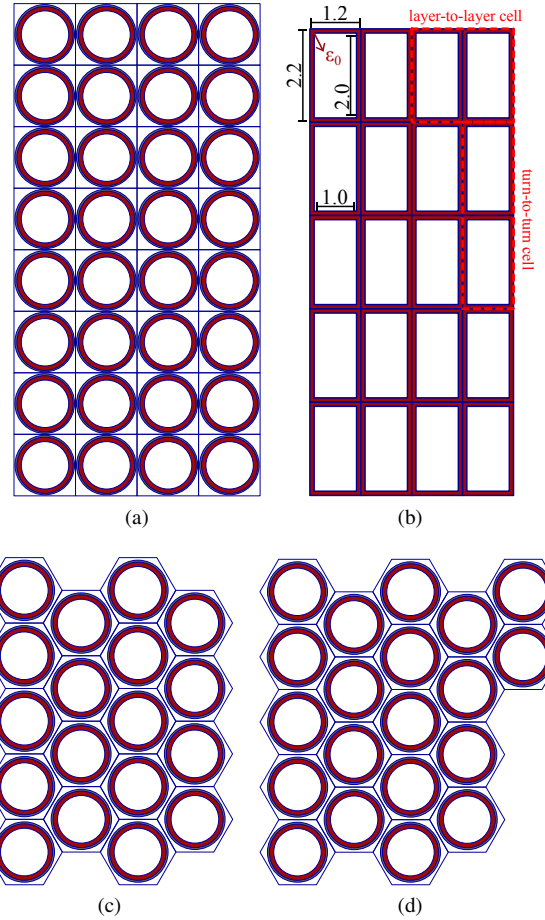


Fig. 4. Application cases (dimensions in mm): (a) 32-turn orthogonal fly-back winding with round conductors (b) 20-turn standard winding with rectangular conductors (c) 18-turn orthocyclic standard winding with round conductors (d) 20-turn orthocyclic fly-back winding with round conductors and an incomplete layer.

IV. APPLICATION

A. Numerical Validation

The four windings shown in Fig 4 are considered to validate the Elementary Neighbor-Conductor Model. The considered windings are: a 32-turn orthogonal fly-back winding with round conductors, a 20-turn standard winding with rectangular conductors, a 18-turn orthocyclic standard winding with round conductors and a 20-turn orthocyclic fly-back winding with round conductors where the last two turns belong to an incomplete layer. In Figs. 4a, 4c and 4d, the conductor characterized in Section III is used.

For simplicity, the windings are fed by sources of 32 V, 20 V, 18 V and 20 V, respectively, so as to satisfy $V_{tt} = 1$ V in all cases. The results of the proposed approach are compared to those obtained by a reference FE model with all turns explicitly discretized (full domains in Fig. 4). A default depth of 1 m is considered for the elementary cells in Fig. 2 and the reference computations of Fig. 4. In all cases, floating potentials i.e., normal electric field with varying potential values, are considered on the domain boundaries. Hereafter, W_{wr} , and C_{wr} are used to express the stored electrical energies and terminal capacitances of the reference cases. Moreover,

the relative error is defined as $\epsilon = |C_{wr} - C_w|/C_{wr}$. The computational times for the FE resolution are denoted t_s and t_{sr} for the proposed approach and the references, respectively, with the speed-up factor given by $sp = t_{sr}/t_s$. All FE computations are carried out with the software Altair Flux™ [24].

First, we consider the 32-turn orthogonal winding shown in Fig 4a, for which the elementary cell proposed in Fig. 2a is used. The reference case leads to a total of 140441 unknowns in the FE problem with a total energy of $W_{wr} = 40.238$ nJ. By applying (7), the resulting terminal capacitance is $C_{wr} = 78.591$ pF. In the homogenized case, the number of unknowns is reduced to 9329, which is approximately 1/16th of the reference unknowns. In general, the number of unknowns is reduced proportionally to the number of non-treated turns, if the same meshing conditions are kept. Via the elementary cell the stored energy in the winding and the terminal capacitance are $W_w = 40.286$ nJ and $C_w = 78.683$ pF, respectively, where C_w has an excellent agreement compared to C_{wr} with relative error $\epsilon = 0.11\%$.

With the objective of treating non-round conductors as well, we consider the 20-turn standard winding with rectangular conductors shown in Fig. 4b. Each turn (rectangle of 1.2 mm by 2.2 mm) comprises the conductor and one layer of insulation around it. The relative permittivity of the insulation is $\epsilon_r = 1$ with $\lambda = 0.76$. In the reference case, the stored energy is $W_{wr} = 23.929$ nJ, which through (7) results in a winding capacitance of $C_{wr} = 119.645$ pF. As for the homogenized case, two different elementary cells are considered to account for the turn-to-turn and layer-to-layer effects. By means of (10), the stored energy in the homogenized approach is $W_w = 23.959$ nJ. The homogenized terminal capacitance is then $C_w = 119.796$ pF, which leads to a relative error of $\epsilon = 0.13\%$.

The windings in Figs. 4c and 4d have an orthocyclic disposition with standard and fly-back connections, respectively. In both cases, the elementary cell of Fig. 2b is used for the homogenized estimation. The reference FE computations for the 18-turn winding yield a stored electrical energy $W_{wr} = 8.061$ nJ with a corresponding terminal capacitance $C_{wr} = 49.759$ pF. In the homogenized model, the stored electrical energy in the cell is $W_{tl} = 79.920$ pJ. Applying (14) together with (15), the stored electrical energy in the winding is $W_w = 8.211$ nJ. Thus, the homogenized winding capacitance results in $C_w = 50.684$ pF; value that agrees very well with the reference and results in a relative error of $\epsilon = 1.86\%$. Note that in this case the relative error is slightly higher since the model uses the voltage approximation given by (14).

As for the 20-turn winding in Fig. 4d, the reference FE computations lead to a stored energy and a winding capacitance of $W_{wr} = 7.250$ nJ and $C_{wr} = 36.250$ pF. The stored energy in the homogenized cell is $W_{tl} = 559.441$ pJ. This time, the stored energy in the winding is obtained with (12) plus the contribution of the additional cell in the incomplete layer (i.e. $N_t(N_t - 1)W_c + W_c$). Hence, the homogenized terminal capacitance is $C_w = 36.361$ pF with relative error of $\epsilon = 0.31\%$, which is again in excellent agreement

TABLE I
RESULTS OF THE ELEMENTARY NEIGHBOR-CONDUCTOR MODEL:
PLANAR CASE

Case	C_{wr} (pF)	C_w (pF)	ϵ (%)
a	78.591	78.683	0.11
b	119.645	119.796	0.13
c	49.759	50.684	1.86
d	36.250	36.361	0.31

TABLE II
COMPARISON OF THE COMPUTATIONAL TIMES: PLANAR CASE

Case	t_{sr} (s)	t_s (s)	sp
a	3.301	0.423	7.8
b	0.556	0.322	1.73
c	1.073	0.378	2.84
d	1.217	0.378	3.93

TABLE III
RESULTS OF THE ELEMENTARY NEIGHBOR-CONDUCTOR MODEL:
AXISYMMETRIC CASE

Case	r_s (mm)	r_e (mm)	C_{wr} (pF)	C_w (pF)	ϵ (%)
a	1.525	2.793	1.066	1.067	0.09
b	0	4.8	1.803	1.804	0.11
c	1.302	2.580	0.607	0.618	1.81
d	1.302	2.727	0.456	0.459	0.66

compared to the reference. If an incomplete winding with standard connection is considered, special attention must be given to the position in terms of the trio q for the incomplete layer. Table I summarizes the obtained terminal capacitances for the windings in Fig. 4.

Table II compares the computational times obtained with the Elementary Neighbor-Conductor Model t_s and the references t_{sr} , including the respective speed-up factors sp . In case b, t_s includes both the resolution the of the turn-to-turn and layer-to-layer elementary cells. Note that the speed-up factor is dependent on the number of turns in the winding and thus it reaches its highest value in Case a for the 32-turn winding. Commonly, windings in real-life devices comprise significantly more turns that the ones considered in Fig. 4 and therefore increased speed-up factors should be expected in such cases.

The axisymmetric case of the windings in Fig. 4 is considered as well. Thus, the reference simulations are recalculated. As for the proposed model, there is no need to run a new FE resolution on the elementary cell, since the aforementioned energies W_w can be transformed into their axisymmetric counterpart through the multiplication by κ . The results are presented in Table III with the corresponding values of r_s and r_e . In the case of the incomplete winding (Fig. 4d), r_e is measured until the middle of the last layer to compensate the lack of turns. Excellent results are found in all cases compared to the corresponding references. The computational times and speed-up factors obtained with the axisymmetric case are similar to those of the planar case showed in Table II.

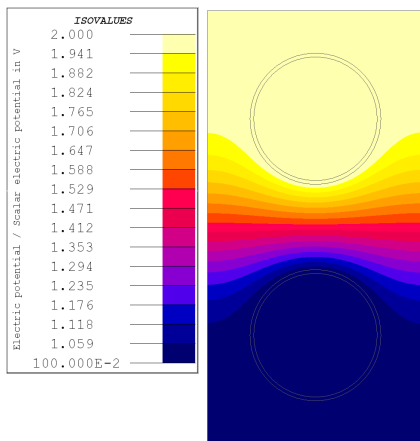


Fig. 5. Potential distribution in the elementary cell of the experimental test case.

B. Experimental Validation

To validate the accuracy of the Elementary Neighbor-Conductor Model, the experimental results measured for a single-layer air-core inductor in [12] are considered. The winding comprises 33 turns of AWG-17 wire with inner diameter 1.15 mm and outer diameter 1.22 mm. The former describes the conductive surface, whereas the latter adds one dielectric layer of $\epsilon_r = 3.3$. The conductor is wound around a PVC bobbin of diameter 24 mm and length 65 mm. The pitch length is set to 2.013 mm. For such prototype, the impedance is measured with a HP4194A impedance/gain analyzer at a frequency of 200 Hz. The measured terminal capacitance is $C_{wr} = 37.55$ fF [12].

The elementary cell is thus defined with an orthogonal disposition, $r_c = 0.575$ mm, $r_1 = 0.61$ mm and $\lambda = 0.256$, following the notation of Section III. The terminal voltage is fixed to $V_T = 33$ V, so that $V_{tt} = 1$ V. The potential distribution in the elementary cell is shown in Figure 5. The winding starting and ending points to define the coordinate transformation factor are $r_s = 11.603$ mm and $r_e = 13.617$ mm. Since the winding comprises a single layer, only the first part of the right-hand side of (9) or (10) is required, evidently with $N_l = 1$. By applying (9) or (10) multiplied by κ , the electrostatic energy stored in the inductor is $W_w = \kappa(N_t - 1)W_{tt} = 1.979$ nJ. Thus, the homogenized terminal capacitance is $C_w = 36.349$ fF. Such value agrees very well with the measured one with a relative error of 3.2%. Note that the Elementary Neighbor-Conductor Model provides better accuracy than the analytic method proposed in [12], which leads to a relative error of 4.8%.

For the sake of completion, the full electrostatic axisymmetric FE model is solved as well with the same imposed potentials, i.e., $V_T = 33$ V, so that $V_{tt} = 1$ V. With such model, the stored electrostatic energy stored in the winding is $W_w = 19.902$ pJ and the corresponding terminal capacitance is $C_w = 36.55$ pJ, leading to a relative error of 2.66%.

V. CONCLUSIONS

A homogenization approach has been proposed for the terminal-capacitance computation of multi-turn windings in

electrostatics FE problems. It estimates the winding capacitance based on an elementary cell that characterizes the regions where the electrostatic energy is concentrated, without describing the full winding in the FE problem. Windings with orthogonal or orthocyclic disposition, fly-back or standard connection, and arbitrary cross-section can be treated with the proposed approaches. In all considered cases, excellent accuracy, compared to both numerical and experimental references, and reduced computational cost is achieved.

The proposed method can be extended to 3-D cells. In such case, the potential distribution along the third axis must be known before the electrostatic resolution. Those values can be obtained by an electrokinetic FE precomputation on the cell. With regard to the frequency, it is important to notice that the proposed model assumes, as every other electrostatic approach, a linear distribution of the voltage across the winding turns. This assumption holds up to a frequency threshold that requires to be estimated on a case-to-case basis. Beyond such limit, other modeling techniques (e.g., higher order approximations) have to be considered.

APPENDIX A

Equation (14) estimates a generalized voltage between the three turns comprised in the orthocyclic elementary cell. Analogous to (6), it represents a linear variation of the voltage depending on the considered trio q , i.e.,

$$V'_{ls} = (Aq - B) \frac{V_T}{N_c}, \quad (17)$$

with A and B the constants to be found. In detail, what such generalized voltage represents is the increase in the stored energy in the cell as v_C changes depending on the considered trio. Therefore, in the performed numerical simulations, v_C changed according to the trio $q = 1, 2, 3, \dots$ and then the stored energy was computed for each case. Those energy values were normalized with respect to the case with $q = 1$, since the objective of the approach is to run the simulations on the cells only once. As a result of the normalization, the rate of change of the squared equivalent-voltage as a function of q is obtained. A simple linear fitting gives the constant values A and B in (17). As long as the shape of the elementary cell is preserved, the proposed equation is valid for any conductor radius, fill factor and number of insulation layers.

REFERENCES

- [1] N. B. Chagas and T. B. Marchesan, "Analytical Calculation of Static Capacitance for High-Frequency Inductors and Transformers," *IEEE Trans. Power Electron.*, vol. 34, no. 2, pp. 1672-1682, Feb. 2019.
- [2] M. Ishigaki, J. Shin and E. M. Dede, "A Novel Soft Switching Bidirectional DC-DC Converter Using Magnetic and Capacitive Hybrid Power Transfer," *IEEE Trans. Power Electron.*, vol. 32, no. 9, pp. 6961-6970, Sept. 2017.
- [3] M. A. Saket, N. Shafiei and M. Ordóñez, "LLC Converters With Planar Transformers: Issues and Mitigation," *IEEE Trans. Power Electron.*, vol. 32, no. 6, pp. 4524-4542, June 2017.
- [4] Z. De Grève, O. Deblecker and J. Lobry, "Numerical Modeling of Capacitive Effects in HF Multiwinding Transformers—Part I: A Rigorous Formalism Based on the Electrostatic Equations," *IEEE Trans. Magn.*, vol. 49, no. 5, pp. 2017-2020, May 2013.
- [5] Y. Zhao and W. N. Fu, "A New Stable Full-Wave Maxwell Solver for All Frequencies," *IEEE Trans. Magn.*, vol. 53, no. 6, pp. 1-4, June 2017.

- [6] R. Hiptmair, F. Kramer and J. Ostrowski, "A Robust Maxwell Formulation for All Frequencies," *IEEE Trans. Magn.*, vol. 44, no. 6, pp. 682-685, June 2008.
- [7] M. Eller, S. Reitzinger, S. Schöps, and S. Zaglmayr, "A Symmetric Low-Frequency Stable Broadband Maxwell Formulation for Industrial Applications," *SIAM Journal on Scientific Computing*, 39:4, B703-B731, 2017.
- [8] W. N. Fu, Y. Zhao, S. L. Ho and P. Zhou, "An Electromagnetic Field and Electric Circuit Coupled Method for Solid Conductors in 3-D Finite-Element Method," *IEEE Trans. Magn.*, vol. 52, no. 3, pp. 1-4, March 2016.
- [9] S. Koch, H. Schneider and T. Weiland, "A Low-Frequency Approximation to the Maxwell Equations Simultaneously Considering Inductive and Capacitive Phenomena," *IEEE Trans. Magn.*, vol. 48, no. 2, pp. 511-514, Feb. 2012.
- [10] P. Dular, R. V. Sabariego and P. Kuo-Peng, "Three-dimensional finite element modeling of inductive and capacitive effects in micro-coils," *COMPEL - The international journal for computation and mathematics in electrical and electronic engineering*, Vol. 25 No. 3, pp. 642-651, 2006.
- [11] J. Biela and J. W. Kolar, "Using Transformer Parasitics for Resonant Converters—A Review of the Calculation of the Stray Capacitance of Transformers," *IEEE Trans. Ind. Appl.*, vol. 44, no. 1, pp. 223-233, Jan.-Feb. 2008.
- [12] A. Ayachit and M. K. Kazimierczuk, "Self-Capacitance of Single-Layer Inductors With Separation Between Conductor Turns," *IEEE Trans. Electromagn. Compat.*, vol. 59, no. 5, pp. 1642-1645, Oct. 2017.
- [13] C. Liu, L. Qi, X. Cui and X. Wei, "A Terminal Capacitance Method for Analyzing Global Capacitive Effects of Magnetic Components," *IEEE Trans. Electromagn. Compat.*, vol. 59, no. 4, pp. 1161-1170, Aug. 2017.
- [14] J. Zhang *et al.*, "Analysis of Inter-Turn Insulation of High Voltage Electrical Machine by Using Multi-Conductor Transmission Line Model," *IEEE Trans. Magn.*, vol. 49, no. 5, pp. 1905-1908, May 2013.
- [15] M. Jaritz, A. Hillers and J. Biela, "General Analytical Model for the Thermal Resistance of Windings Made of Solid or Litz Wire," *IEEE Trans. Power Electron.*, vol. 34, no. 1, pp. 668-684, Jan. 2019.
- [16] X. Liu, Y. Wang, J. Zhu, Y. Guo, G. Lei and C. Liu, "Calculation of Capacitance in High-Frequency Transformer Windings," *IEEE Trans. Magn.*, vol. 52, no. 7, pp. 1-4, July 2016.
- [17] Z. Shen, H. Wang, Y. Shen, Z. Qin and F. Blaabjerg, "An Improved Stray Capacitance Model for Inductors," *IEEE Trans. Power Electron.*, vol. 34, no. 11, pp. 11153-11170, Nov. 2019.
- [18] B. Wu, X. Zhang, X. Liu and C. He, "An Analytical Model for Predicting the Self-Capacitance of Multi-Layer Circular-Section Induction Coils," *IEEE Trans. Magn.*, vol. 54, no. 5, pp. 1-7, May 2018.
- [19] M. Aghaei and S. Kaboli, "On the Effect of Disorder on Stray Capacitance of Transformer Winding in High-Voltage Power Supplies," *IEEE Trans. Ind. Electron.*, vol. 64, no. 5, pp. 3608-3618, May 2017.
- [20] A. Massarini and M. K. Kazimierczuk, "Self-capacitance of inductors," *IEEE Trans. Power Electron.*, vol. 12, no. 4, pp. 671-676, July 1997.
- [21] Z. De Grève, O. Deblecker and J. Lobry, "Numerical Modeling of Capacitive Effects in HF Multiwinding Transformers—Part II: Identification Using the Finite-Element Method," *IEEE Trans. Magn.*, vol. 49, no. 5, pp. 2021-2024, May 2013.
- [22] L. Deng *et al.*, "Modeling and Analysis of Parasitic Capacitance of Secondary Winding in High-Frequency High-Voltage Transformer Using Finite-Element Method," *IEEE Trans. Appl. Supercond.*, vol. 28, no. 3, pp. 1-5, April 2018.
- [23] Z. De Grève, O. Deblecker, J. Lobry and G. Meunier, "Homogenization of the Thin Dielectric Layers of Wound Components for the Computation of the Parasitic Capacitances in 2-D FE Electrostatics," *IEEE Trans. Magn.*, vol. 49, no. 5, pp. 1849-1852, May 2013.
- [24] *Altair Flux*TM. (2019.1), Altair Engineering. Accessed: Feb. 20, 2020. [Online]. Available: <https://www.altair.com/flux/>